
Seasonal and subseasonal climate changes recorded in laminated diatom ooze sediments, Adélie Land, East Antarctica

D. Denis^{1*}, X. Crosta¹, S. Zaragosi¹, O. Romero², B. Martin¹, V. Mas¹⁻³

1 UMR-CNRS 5805 EPOC, université Bordeaux 1, av. des Facultés, 33405 Talence cedex, France

2 Department of Geosciences and RCOM, University of Bremen, PO Box 330440, 28334 Bremen, Germany

3 IFREMER, Géosciences Marines, Laboratoire Environnements Sédimentaires, BP70, 29280 Plouzané Cedex, France.

*: Corresponding author : d.denis@epoc.u-bordeaux1.fr

Abstract:

A 40 m long sediment core covering the 1000–9600 years BP period was retrieved from the Dumont d'Urville Trough off Adélie Land, East Antarctica, during the MD 130–Images X-CADO cruise. This sedimentary sequence allows the documentation of changes in climate seasonality during the Holocene. Here we show preliminary results of diatom communities, lithic grain distribution and titanium content measured on two 30 cm long sequences of thin sections. The two sequences originate from two different climate regimes, the colder Neoglacial and the warmer Hypsithermal. Proxies were measured at microscale resolution on 25 laminations for the Neoglacial and 14 laminations for the Hypsithermal. The two sequences reveal alternating light-green and dark-green laminae. Light laminae result from low terrigenous input and high sea-ice edge diatom fluxes and are interpreted to represent the spring season. Dark laminae result from high terrigenous input mixed with a diversified open ocean diatom flora and are interpreted to represent the summer–autumn season. The two sequences therefore resolve annual couplets composed of one light plus one dark lamina. Variations in the relative thickness of laminations and annual couplets, associated with diatom assemblage changes, are observed in each sequence and between the two sequences giving information on interannual to millennial changes in environmental conditions.

Keywords: Adélie Land • Holocene • laminated sediments • diatom ooze • seasonality • sea ice • East Antarctica

48 Based on ice core records (Masson *et al.*, 2000; NGICP members, 2004), the Holocene period
49 was believed rather stable in comparison to the last glacial period. However recent paleo-
50 oceanographic investigations have revealed rapid and large amplitude variations in the North
51 Atlantic (De Menocal *et al.*, 2000; Bond *et al.*, 2001) and the Southern Ocean (Hodell *et al.*,
52 2001; Nielsen *et al.*, 2004). Sites of high sediment accumulation are therefore necessary to
53 document these variations and to understand their frequency and origin. In that perspective,
54 Antarctic inner shelf basins that present laminated sediments allow annual to sub-seasonal
55 reconstructions of Holocene oceanographic and climatic conditions, which may help to
56 understand better both the interactions between Antarctic atmospheric-oceanic-cryospheric-
57 sea ice processes, deep ocean circulation and teleconnections between high- and low latitudes.
58 Most of the studies aimed at deciphering the signal recorded in laminations originate from the
59 Antarctic Peninsula (e.g. Pike *et al.*, 2001; Bahk *et al.*, 2003; Leventer *et al.*, 2002; Maddison
60 *et al.*, 2005) and the Mac.Robertson Shelf (Stickley *et al.*, 2005). Nonetheless, evidence for
61 strong Antarctic regional heterogeneities in recent climate changes (Jones *et al.*, 1993; King *et al.*
62 *et al.*, 2003) call for additional sedimentary records in order to provide a more comprehensive
63 view of past climate dynamics at high southern latitudes. The Adélie Land region in the East
64 Antarctica Margin (EAM) has received little attention so far despite evidences for very high
65 sediment accumulation (Leventer *et al.*, submitted). Core MD03-2601 from the Dumont
66 d'Urville Trough is a 40 m-long sequence of laminated diatom ooze that covers the Holocene.
67 Investigation of diatom communities, lithic grain distribution and titanium content at micro-
68 scale resolution on two 30 cm-long laminated sequences aimed to document (1) the nature of
69 the signal preserved in the laminations and (2) whether laminations may be used here to track
70 climate change at the interannual timescale.

71

72 2. Oceanographic Setting

73 The SE-NW oriented Dumont d'Urville Trough off Adélie Land is located on the EAM
74 (Figure 1). It is composed of a succession of glacial depressions enclosed between the Dibble
75 Bank to the west and Adélie Bank to the East. Core MD03-2601 (66°03.07'S; 138°33.43'E;
76 746 m water depth) was recovered from the slope of a small depression located ~ 60 km off
77 the Adélie Land coast. This region is influenced by three water masses (Bindoff, 2001): the
78 Antarctic Coastal Current (ACC) which flows westward at the surface (Figure 1), the
79 Modified Circumpolar Deep Water (MCDW) which upwells at the Antarctic Divergence, and
80 the High Salinity Shelf Water (HSSW) formed by brine-rejection during winter sea ice
81 formation and cooling of the MCDW, which flows northward as part of the AABW (Harris,

82 2000). The Adélie Land region is dissected by several small glaciers (Figure 1) injecting
83 freshwater and terrigenous particles in the coastal area although these small glaciers have
84 much less influence than the larger Mertz Glacier located few degrees to the East (Escutia *et*
85 *al.*, 2003). Sea ice is present ~9 months per year over the core site (Schweitzer, 1995) with
86 more open marine conditions between January and March. Sea ice advances rapidly from
87 April to June to reach its maximum extension between July and September, then retreats
88 slowly during spring melting to attain its minimum extent during February. The Marginal Ice
89 Zone is believed to be macro- and micro-nutrient rich, and ice melting produces a stratified
90 stable environment favourable for diatom blooms (Leventer *et al.*, 1992).

91

92 3. Material and Methods

93 3. 1. Material and core stratigraphy

94 Core MD03-2601 was collected using the MDII Calypso piston corer during the MD130-
95 *Images X* CADO cruise in 2003. This 40.24 m long sequence of diatom ooze alternates between
96 laminated and massive facies, and does not show any obvious visual disturbance.
97 Stratigraphic control is based on five AMS ¹⁴C dates on humic acid (Crosta *et al.*, 2005) that
98 were subsequently corrected by a marine reservoir age of 1300 years (Ingólfsson *et al.*, 1998).
99 The core covers the period from 9600 to 1000 yr BP. Diatom census counts and $\delta^{15}\text{N}$ and $\delta^{13}\text{C}$
100 investigations (Crosta *et al.*, 2005) have shown that the Holocene period off Adélie Land can
101 be divided into two different climatic phases: a colder Neoglacial (after 4000 yr BP), and a
102 warm Hypsithermal (4000 to 9600 yr BP) which contains a cooling event (6350 to 8000 yr
103 BP).

104

105 3.2. Laboratory procedures

106 Laboratory procedures involve preparations for macro-scale investigations on half-
107 core sections and for micro-scale analyses on thin sections.

108 Titanium content (Ti) expressed in counts per second (cps) was measured on half-core
109 sections at 2 cm spacing along the entire core and at 2 mm spacing on the studied sections on
110 the Bremen University CORTEX XRF core-scanner following Jansen *et al.* (1998) method.
111 Daily calibration of the XRF core-scanner precluded drift over time, thus ensuring low
112 standard deviations of the data. Titanium is believed to be of terrigenous origin as this
113 element does not participate in biological and diagenetic cycles, in contrast to iron and
114 aluminium (Taylor and McLennan, 1985; Yarincik and Murray, 2000). Aluminium, which is

115 actively uptaken and accumulated by diatoms, cannot be applied here to normalize Ti values
116 (Van Bennekom *et al.*, 1989; Moran and Moore, 1992).

117 Positive X-ray pictures of half-core sections were done using the SCOPIX image-
118 processing tool (Migeon *et al.*, 1999). Variations in grey levels indicate changes in the
119 sediment density and thus composition. The light and dark laminations observed here
120 correspond to sediment layers of low and high density, respectively.

121 Based on X-ray pictures, we determined the distribution and thickness of laminations
122 along the entire core (Figure 2). We used a slightly modified technique from Francus *et al.*
123 (2002) which involves drawing a suite of ellipses representative of each lamina and
124 calculation of the distribution and thickness of laminae based on the ellipses in Scion Image®.
125 This technique was applied to laminae only because sub-laminae are difficult to distinguish
126 on X-ray pictures. This approach helped us to sample two ~30 cm-long sections of
127 continuously laminated sediment. Section 5 (619-648.5 cm) originates from the Neoglacial
128 while section 13 (1880.8-1910.7 cm) comes from the Hypsithermal.

129 Each lamina observed on X-ray pictures from sections 5 and 13 was sampled for
130 diatom census counts and bulk isotopic ratios. Permanent slides were mounted following the
131 procedure of Rathburn *et al.* (1997). This sampling strategy that takes the sediment over the
132 entire thickness of the half-core sections cannot give access to diatom successions at the
133 lamination scale because laminae are here inclined in both the horizontal and vertical plans.
134 Such diatom census counts are, however, essential to interpret diatom assemblages at micro-
135 scale on the thin sections.

136

137 Three thin sections (TS) were made for each period (TS 1, 2, 3 for core section 5 and
138 TS 4, 5, 6 for core section 13) using the impregnating method detailed in Zaragosi *et al.*
139 (submitted). The goal of this technique is to embed a large sediment volume into a permanent
140 medium without disturbing the sediment structure. The resulting thin sections (TS) are used
141 here to document variations in the biogenic and lithogenic content.

142 Optical observations were conducted on the TS using an Olympus BH2 light
143 microscope at magnification of x250 and x500 to determine diatom community changes with
144 a focus on the relative importance of dominant species. Diatom census counts along the entire
145 core (Crosta *et al.*, 2005) and within each lamina over the studied sections give us
146 complementary insight on diatom assemblages and dominant species at decadal to sub-
147 decadal scales, which ascertains diatom identification on the TS.

148 Detrital material was similarly studied on the TS to determine (1) the mineral type via
149 polarised light and (2) the distribution and number of lithics particles as grain number per
150 mm² using an imagery system composed of a LEICA DM600B Digital microscope and Leica
151 QWin 3.0 software. We conducted image analysis on 2.5-3.5 cm² TS areas, later-on referred
152 to Photomosaic (PM) (Figure 4). Because of the homogeneous amorphous matrix of the
153 diatom ooze sediment and of the impregnating Epoxy resin, the sediment matrix appeared
154 darker than the clastic grains in the analyzed-polarized light. The picture processing method,
155 detailed in Francus *et al.* (1998), counts all the grains present in the area and estimates several
156 characteristics as surface, width and length of the lithic grain. Two slides (TS2 and TS3) with
157 very cottony texture did not allow coherent image acquisition and were not used in the
158 calculations.

159

160 4. Results

161 4. 1. General observations

162 Due to the sediment composition, laminations are almost invisible to the naked eye on half-
163 core sections. They are however visualized on X-ray images as light and dark layers and on
164 TS as light and brown layers. We will hereafter refer to light and dark laminae which together
165 form a couplet.

166 Mean thicknesses of light and dark laminations are 0.7 cm (n = 937, $\sigma = 0.4$) and 1.12 cm (n =
167 1018, $\sigma = 1.22$), respectively (Figure 2). Light and dark lamination thickness and lamination
168 number reveals no obvious trend with depth but rather cyclic variations whereas thickness of
169 light laminations shows a slight decrease with depth.

170 Generally, X-ray images and TS show gradational colour contact between a light lamina and
171 the overlying dark lamina and sharp colour contact from a dark to the overlying light lamina.
172 Microscopic observations on TS reveal that light laminations are mainly composed of
173 biogenic debris whereas dark laminations are composed of a mixture of biogenic and detrital
174 debris, the latter ones being mainly clay and silt. Petrographic observations indicate that the
175 clastic grains are mainly quartz. Only observable on TS, thin light laminae, called sub-
176 laminae, are found in dark laminations.

177

178 4. 2. Section 5: Neoglacial period

179 Twenty-five laminations and four sub-laminations are distinguished on TS 1, 2 and 3 that
180 represent a ~30 cm-long sequence of undisturbed sediment within section 5 (see figure 4a for
181 TS location) . These laminations include 12 lights, 11 darks and 2 transitional laminae with

182 average thicknesses of 1.1 cm ($\sigma = 0.8$), 0.8 cm ($\sigma = 0.8$) and 0.4 cm ($\sigma = 0.03$) respectively.
183 The mean thickness of a couplet reaches 2.1 cm ($n = 10$, $\sigma = 1.4$).

184

185 4. 2. 1. Diatom assemblages

186 Diatom census counts performed between 608 cm and 670 cm ($n = 50$) show few dominant
187 species among a highly diverse diatom community (~50 species), thus confirming results
188 from lower resolution diatom counts (Crosta *et al.*, 2005). In section 5, *Fragilariopsis curta*
189 and *Chaetoceros* resting spores (CRS), mainly *Hyalochaete Chaetoceros neglectus*, represent
190 the dominant species with 26% and 19% respectively. They are accompanied by a set of
191 subordinate species or species groups such as other cryophilic *Fragilariopsis* species (12%),
192 *F. rhombica* (10%), *F. kerguelensis* (8%), large centric species thriving in cold waters (8%),
193 *Thalassiosira antarctica* (6%), *Phaeoceros* vegetative cells (5%), *Corethron pennatum* +
194 rhizosolenoid species (4%), and needle-like species mainly represented by *Thalassiothrix*
195 *antarctica* (2%), (Figure 3a).

196 Qualitative examinations of diatom assemblages on the TS demonstrate the same dominant
197 species as mentioned above. These investigations, however, show the fine distribution of the
198 diatom species that was invisible in the stepwise sampling. As a general statement, diatom
199 distribution follows the colour changes of the laminations with a gradational evolution in the
200 assemblages from light to dark laminae and an abrupt change from dark to light laminae. A
201 close investigation depicts the following five main diatom assemblages, labelled A-B for the
202 ones occurring in the light laminae and D-E-F for the ones encountered in dark laminae
203 (Figure 3a and 5).

204 Assemblage type A is characterised by a co-dominance of *F. curta* plus other cryophilic
205 *Fragilariopsis* species and CRS plus vegetative *Phaeoceros* sp. and *C. pennatum*.
206 *Chaetoceros* RS relative abundance increases progressively toward the top of laminae while
207 cryophilic *Fragilariopsis* species dominance decreases (Figure 3a). Assemblage type B is
208 similar to assemblage type A with greater abundances of *C. pennatum*, rhizosolenoids and
209 vegetative *Phaeoceros* sp. Assemblage type B becomes nearly bispecific in *C. pennatum* and
210 rhizosolenoids in one occasion at the top of light lamination number five (Figure 3a). We
211 counted 11 light laminae in the three TS of section 5, from which 3 laminae are characterized
212 by assemblage type A, 5 laminae by assemblage type B and 4 laminae by a slow transition
213 from assemblage type A to assemblage type B. The third and the ninth light laminae
214 contained more CRS.

215 Assemblage type D shows a mixed flora composed of *F. kerguelensis*, CRS, *T. antarctica*,
216 large centric species, *Phaeoceros* sp., and *C. pennatum*. Assemblage type E is similar to
217 assemblage type D but with greater presence of *T. antarctica*. Assemblage type F also
218 resembles assemblage type D but with a greater dominance of needle-like species (Figure 3a).
219 We counted 11 dark laminations, from which 7 of them are composed of the assemblage type
220 D. The other dark laminations display a succession of assemblage types. Four laminations
221 show a slow evolution from assemblage type E to assemblage type F, 1 lamination from
222 assemblage type D to assemblage type F, and 1 lamination from assemblage type D to
223 assemblage type E to assemblage type F (Figure 3a). Diatoms at the top of the dark
224 laminations generally show a higher degree of silicification (Figure 5). Complex dark
225 laminations are encountered in couplets number five to ten in which light laminations also
226 demonstrate a more complex structure. Transitional laminations between the light and the
227 overlying dark lamination and showing a mixture of assemblage types A, B and D
228 characteristics are also present here.

229

230

4. 2. 2. detrital content

231 Titanium content is correlated to density changes visualized by X-ray photography with lower
232 Ti content in light laminations than in dark laminations with mean values of 11.6 and 13.7 cps
233 respectively (Figure 4a). Titanium content is similarly correlated to TS colour changes even
234 though some variability is encountered within each lamina. We used the Wilcoxon-Mann-
235 Whitney (WMW) test to determine whether the Ti content is significantly different in light
236 and dark laminations. Briefly, the WMW is a non parametric variance analysis test adapted
237 for small data set ($n_{\text{light}} = 45$, $n_{\text{dark}} = 47$, here) (Saporta, 1990). This test determines whether Ti
238 values are randomly distributed or organized according to different populations (light and
239 dark laminations). At the 1% confidence level, the WMW test yields $H_{\text{Ti content}}$ value of 4.32
240 that is superior to the rejection threshold of 2.58. This demonstrates that different Ti content
241 indeed prevails in light and dark laminations and that intra-couplet differences are greater than
242 homochromic inter-couplet differences.

243 Determination of grain distribution and characteristics was only possible on TS 1 within two
244 study zones: PM 1 and 2 (Figure 4a). The digital approach recognizes grains with diameter
245 greater than 5 μm . In this population, silts are dominant with an unimodal histogram
246 frequency centred at $\sim 10 \mu\text{m}$ of diameter. In agreement with the Ti content data, the number
247 of lithic grains (GN) is generally lower in light ($n_{\text{laminae}} = 4$) than in dark laminae ($n_{\text{laminae}} = 5$)
248 with mean values of 303 and 548 grains per mm^2 , respectively (Figure 4a). We ascertained

249 the significance of different grain populations in light versus dark laminations through the
250 WMW statistic test. At the 1% confidence level, the WMW test yields a H_{GN} value of 2.84
251 superior to the rejection threshold of 2.58 ($n_{light} = 23$, $n_{dark} = 43$). Different GN thus prevails
252 in light and dark laminations indicating that intra-couplet differences are greater than inter-
253 couplet differences between laminae of the same colour.

254

255 4. 3. Section 13: Hypsithermal period

256 Fourteen laminations and twenty-six sub-laminations were observed in section 13 (TS 4, 5, 6)
257 (see Figure 4b for TS location). The laminations divide up into 5 lights, 6 darks and 3
258 transitional laminae with respective thicknesses of 0.7 cm ($\sigma = 0.1$ cm), 3.6 cm ($\sigma = 1.8$ cm)
259 and 0.6 cm ($\sigma = 0.2$ cm) yielding an average thickness of 4.6 cm ($\sigma = 1.6$) for the couplets.
260 Thickness of sub-laminae varies between 0.1 and 2.1 mm ($n = 26$, mean = 1 mm, $\sigma = 0.6$
261 mm).

262

263 4. 3. 1. Diatom assemblages

264 Diatom census counts performed between 1858 cm and 1919 cm ($n = 62$) evidence the same
265 diatom species as in section 5 but with an important shift in dominance. *Chaetoceros* resting
266 spores (22%), *F. kerguelensis* (19%), *F. rhombica* (15%) and *T. antarctica* (11%) are more
267 abundant and are accompanied by a suite of subordinate species such as large centric diatoms
268 (9%), *F. curta* (9%), other cryophilic *Fragilariopsis* diatoms (8%), *Phaeoceros* vegetative
269 cells (4%), needle-like species (2%) and *C. pennatum* and rhizosolenoids (1%) (Figure 3b).

270 Qualitative examinations of diatom assemblages on the TS demonstrate the same dominant
271 species as mentioned above with a gradational evolution of the assemblages from light to dark
272 laminae and an abrupt change from dark to light laminae. Three main assemblages are
273 documented: assemblages type C in the light laminae and assemblages type E and F in the
274 dark laminae (Figure 5).

275 Assemblage type C is mainly composed of *F. rhombica* associated to cryophilic
276 *Fragilariopsis* sp., *F. kerguelensis* and CRS. The relative occurrence of CRS increases from
277 bottom to top of the laminae. Out of five light laminations analyzed on the TS taken from
278 section 13, four are composed of assemblage type C. The last lamination is represented by the
279 bi-specific assemblage type B defined before (Figure 3b).

280 Dark laminations are characterized by the above-described assemblage types E and F. Out of
281 six dark laminations, five are characterized by assemblage type E while the last lamination is
282 composed of assemblage type F. We noted the presence of three transitional laminae, showing

283 a mixture of assemblage types C, B and D in the lower part of the TS sequence (Figure 3b).
284 We also noted that dark laminations numbers 1 and 4 present greater relative abundances of
285 CRS and higher frustule silicification (Figure 5).
286 Twenty-six sub-laminae appear as thin light laminae within dark laminations with upper and
287 lower sharp contacts. Diatom examinations evidence three diatom assemblage types. Two are
288 near monospecific assemblages, composed of *T. antarctica* (n = 8) or rhizosolenoids (n = 3)
289 and referred to Ta and Rh respectively (Figure 5). The last one, named P for pulsed event, is
290 similar to assemblage type D (n = 15), (Figure 3b). The Rh sub-laminae appear at the bottom
291 of dark laminations while the Ta sub-laminae generally occur at the top of dark laminations.
292 P sub-laminae are scattered throughout dark laminations. Ta, Rh and P display mean
293 thicknesses of 371 μm ($\sigma = 289 \mu\text{m}$), 860 μm ($\sigma = 470 \mu\text{m}$) and 1300 μm ($\sigma = 460 \mu\text{m}$)
294 respectively. These sub-laminae cannot be interpreted as light laminations because of their
295 specific diatom assemblages and reduced thickness. They conversely represent abrupt events
296 during deposition of the dark laminations.

297

298 4. 3. 2. Detrital content

299 Ti relative concentrations are lower in light laminae than in dark laminae both at the X-ray
300 and TS scale with mean values of 13 and 14 cps respectively (Figure 4b). Digital analysis of
301 grains larger than 5 μm indicates dominance of the silt fraction with a unimodal histogram
302 frequency centred at $\sim 10 \mu\text{m}$ diameter. The number of grains (GN) calculated on 5 PM (figure
303 4b) follows the same pattern as Ti content with mean values of 152 grains per mm^2 in light
304 laminations and 264 grains per mm^2 in dark laminations. At the 1% confidence level, the
305 WMW test yields a $H_{\text{Ti content}}$ value of 1.72, greater than the rejection threshold of 1.64, and a
306 H_{GN} value of 5.61, also superior to the rejection threshold of 2.58 ($n_{\text{light}} = 25$, $n_{\text{dark}} = 111$ for
307 Ti content; $n_{\text{light}} = 58$, $n_{\text{dark}} = 94$ for GN). This demonstrates that different detrital populations
308 prevail in light and dark laminations of the sequence studied here and that the intra-couplet
309 differences in Ti content and GN are greater than inter-couplet differences of the same color
310 type lamination.

311

312 5. Discussion

313 The presence of well-preserved frustules of needle-like species and of the easily-dissolved
314 species *C. pennatum* (Beucher *et al.*, 2004) indicates that buried diatom communities are
315 barely influenced by differential preservation, and, thus accurately record surface
316 environment changes. We hereafter use data on detrital content as well as the ecological

317 preferences of dominant species to determine the significance of lamination types and to link
318 their succession to environmental conditions.

319

320 5. 1. Seasonal and sub-seasonal signals

321 5. 1. 1. Light/biogenic laminae

322 Light laminae are characterized by low density, low Ti content and low GN. They are
323 therefore mainly composed of biogenic material, i.e. diatoms. Light laminae are characterized
324 by assemblage types A and C in which cryophilic *Fragilariopsis* species (mainly *F. curta* in
325 section 5 and *F. rhombica* in section 13) and CRS are the co-dominant species groups, with
326 subordinate presence of *C. pennatum* and vegetative *Phaeoceros* sp..

327 *Fragilariopsis curta* and CRS show a preference for stable, stratified waters and sea ice
328 proximity (Leventer, 1991; McMinn and Hodgson, 1993; Crosta *et al.*, 1997) that seeds the
329 surrounding surface water as it melts. This seems also true for *F. rhombica* with the
330 difference that this species thrives in waters slightly warmer than *F. curta* (Armand *et al.*,
331 2005). These conditions are encountered in spring and, when associated with sufficient light
332 and nutrients levels, promote intense diatom blooms. Blooms may eventually deplete the
333 nutrient pool thus leading to CRS formation (Leventer, 1991). We therefore interpret the
334 light/biogenic laminae to represent the spring season. Spring laminae evidence here, however,
335 depart from previous studies in other cores from the EAM (Stickley *et al.*, 2005) and the
336 Antarctic Peninsula (Leventer *et al.*, 2002; Bahk *et al.*, 2003; Maddison *et al.*, 2005) in which
337 the spring season is characterized by greater abundances of CRS (60%). Low CRS occurrence
338 is confirmed by diatom census counts all core long (Crosta *et al.*, 2005) and may result from
339 more oceanic conditions prevailing at the core location. Indeed, presence of *Phaeoceros*
340 vegetative cells suggests an oceanic influence (Maddison, 2005) and *Ch. neglectus* has not
341 been reported to be seeded from sea ice (Garrison *et al.*, 1987; Riaux-Gobin *et al.*, 2003).

342

343 Assemblage type A may be followed by the predominance of migrant species such as *C.*
344 *pennatum* and rhizosolenoids that characterize the diatom assemblage type B. These species
345 thrive normally in open water with little sea ice during the growing season (Fryxell and Hasle,
346 1971) and display positive buoyancy (Crawford, 1995; Leventer *et al.*, 2002; Bahk *et al.*,
347 2003). Out of Antarctica, these species groups were shown to be part of the shade flora which
348 reaches very high biomass at the pycnocline (Kemp *et al.*, 1999). Their record in the sediment
349 was interpreted as an event of rapid sedimentation when the pycnocline weakened (Kemp *et*
350 *al.*, 2000). Increasing occurrence of *C. pennatum* and rhizosolenoids throughout the light

351 laminae suggest here a strengthening of the pycnocline during the spring season thus
352 conducting to increasing biomass accumulation and export after cell senescence. This
353 assemblage therefore may be an indicator of warmer, more oligotrophic, open-water intrusion
354 (Stickley *et al.*, 2005) or reduced wind stress.

355 The diatom succession from cryophilic *Fragilariopsis* species to CRS and finally to migrant
356 species observed here indicates a transition from a cold-stratified environment with extensive
357 sea ice cover at the beginning of the spring season to more open water as temperatures rise
358 with increasing seasonal insolation coupled to a decrease of the nutrient pool. Sea ice
359 persistence implies low terrigenous input from the continent which is additionally diluted by
360 the intense diatom fluxes to the sea-floor.

361

362 5. 1. 2. Dark/terrigenous laminae

363 Dark laminae are characterized by higher density, higher Ti content and higher GN. They are
364 composed of a mixture of biogenic and terrigenous material. Dark laminae are characterized
365 by more diverse diatom assemblages dominated by *F. kerguelensis*, *T. antarctica* and large
366 centric species. These species preferentially thrive in open ocean water and do not support sea
367 ice presence during the growing season (Armand *et al.*, 2005; Crosta *et al.*, 2005). They also
368 exhibit lower nutrient requirements and lower growth rates than bloom-related species
369 (Leventer and Dunbar, 1987; Zielinski and Gersonde, 1997). We interpret these assemblages
370 as representative of summer production in open water when sea ice has retreated and nutrient
371 levels are low, in agreement with previous studies conducted in the EAM (Leventer *et al.*,
372 2002; Bahk *et al.*, 2003; Stickley *et al.*, 2005; Maddison, 2005).

373 *Corethron pennatum* and *Phaeoceros* vegetative cells are less abundant than in light laminae
374 but display larger size and a higher degree of silicification, indicating a slow biomass build-up
375 during the summer months. At the end of summer season, the presence of needle-like species
376 may become predominant to form the assemblage type F. Here again, they may indicate the
377 return of atmospheric perturbations during autumn which disrupt the pycnocline thus
378 exporting downward the shade flora slowly growing at the nutricline (Bahk *et al.*, 2003).

379 Both Neoglacial and Hypsithermal sections display greater GN and Ti content in dark
380 laminations than in light laminations, suggesting higher terrigenous input during dark laminae
381 deposition. In our study area, lithogenic input may have several sources including eolian dust,
382 focusing by deep currents (Presti *et al.*, 2003), glacial runoff and sub-glacial melting (Rignot
383 and Jacobs, 2002). The eolian source, even with melting dirty sea-ice, cannot account for the
384 terrigenous fraction based on its timing. Indeed one would expect greater deposition during

385 spring when sea ice decay releases dust particles. Strong winnowing that transports diatom
386 frustules along with the detrital particles is not coherent with the seasonal and sub-seasonal
387 signature of diatom assemblages. We therefore suggest that glacial and sub-glacial inputs are
388 the dominant detrital sources to our core site and occur mainly during summer/autumn season
389 before the return of sea ice. Material input is primarily controlled by the extent and
390 persistence of sea ice cover with secondary influence of atmospheric conditions. This inferred
391 seasonal cycle in the detrital supply may be affected by the diluting effect of rapid and intense
392 biogenic settling events.

393

394 The described sedimentary record preserves the imprint of seasonal and sub-seasonal
395 biological and sedimentological dynamics with biogenic laminae representing spring fluxes
396 and more terrigenous laminae corresponding to summer/autumn fluxes. The gradational
397 contact between light and overlying dark laminations is due to slow changes in the biological
398 and sedimentological inputs while the sharp contact between dark and overlying light
399 laminations is due to the winter hiatus as annual sea ice reforms. These findings support the
400 interpretation of an annual light-dark couplet.

401

402 5. 1. 3. Sub-laminae

403 Terrigenous laminae may be interrupted by sub-laminae that represent events of rapid
404 biogenic export during summer that dilute the terrigenous fraction. The rhizosolenoids sub-
405 laminae are encountered at the bottom of the dark laminations, therefore occurring at the
406 beginning of summer season. They demonstrate nutrient limitation above a well-defined
407 pycnocline that enhances their development to the detriment of other species. Nutrient
408 limitation may be linked to a pulsed input of oligotrophic warmer water as evidenced in the
409 Mac.Robertson Shelf (Stickley *et al.*, 2005). The abruptness of the Rh events probably
410 records punctual pycnocline breakdown. P sub-laminae, present throughout dark laminations,
411 may indicate short bloom events in response to renewal of the nutrient pool via pulsed
412 resurgence of deep waters. Ta sub-laminae, generally found at the end of summer/autumn
413 season, certainly indicate an environmental stress such as decrease of light level and increase
414 of salinity when sea-ice returns (Leventer *et al.*, 2002; Maddison *et al.*, 2005; Stickley *et al.*,
415 2005). Closer to the Adelie Coast, similar sub-laminae of nearly monospecific *Porosira*
416 *glacialis* RS are found to interrupt dark summer laminations (Maddison, 2005). Although
417 both species are thought to have similar growth requirements (Stickley *et al.*, 2005) and
418 forecast the autumn/winter transition, we show here that *P. glacialis* may thrive at colder

419 temperatures and higher sea ice cover than *T. antarctica* in agreement with their occurrence in
420 surface sediments (Armand *et al.*, 2005). Diatom census counts evidence anti-correlated
421 occurrences of these two species in core MD03-2601 during the Holocene (data not shown)
422 and ascertain the dominance of *T. antarctica* over *P. glacialis* in the TS.

423 The three above-described sub-laminae types record spring/summer transition (Rh), punctual
424 intense summer blooms (P) and autumn/winter transition (Ta). The distribution of the sub-
425 laminae may provide information on atmospheric and oceanic shifts and on sea ice
426 seasonality at the annual scale.

427

428 5. 2. A model of lamina deposition

429 We developed a schematic model to explain the climatic and oceanic conditions leading to the
430 deposition of the laminations (Figure 6). At the beginning of spring, sea ice starts to melt but
431 a still large extent limits continental input to the water column. Sea ice melting creates strong
432 water column stratification while supplying diatoms and macro- and micro-nutrients to the
433 surface waters. The beginning of spring is also a time of decrease in the wind regime, of
434 increase in light levels and of high nutrient content in response to the winter overturning.
435 These factors create a favourable environment supporting an intense bloom of cryophilic
436 pennate diatoms and *Chaetoceros* species. As spring advances, the reduction of sea ice
437 influence and the intense nutrient uptake eventually cause CRS formation. Meanwhile, *C.*
438 *pennatum* and rhizosolenoids slowly build-up high biomass at the well-defined pycnocline.
439 They eventually settle after cell senescence or after episodic pycnocline breakdown. In the
440 Antarctic Peninsula, similar laminations have been interpreted to represent autumn mass
441 sedimentation of diatoms which have grown during the period of summer stratification.
442 Summer stratification is promoted by reduced wind activity and the local ‘island effect’
443 (Amos, 1987; Huntley *et al.*, 1987). In our study area, more oceanic and more chaotic
444 atmospheric conditions (King and Turner, 1997) conducting to less stable surface water layer,
445 explain episodic export events early in the season. High spring primary production in the form
446 of successive diatom blooms and low detrital supply produces thick biogenic spring laminae.
447 As summer approaches, light increases and sea ice disappears driving a transitional diatom
448 assemblage characterized by the appearance of the open water species *F. kerguelensis* and of
449 centric species, mixed with cold water species. At the beginning of summer, punctual
450 pycnocline disruption leads to pulsed exports of rhizosolenoids, imprinted by thin sub-
451 laminae. Dilution of sea ice melt-water reduces water column stratification and increases the
452 depth of the pycnocline. The summer light levels are maximum and nutrient content is

453 maintained via MCDW upwelling. These conditions lead to the development of mixed diatom
454 communities primarily dominated by *F. kerguelensis*, while centric species that present a
455 slower growth rate may become co-dominant as the summer develops. A slower but longer
456 diatom growth during summer than during spring is inferred from the higher silicification
457 degree of *C. pennatum*, vegetative *Phaeoceros* sp. and *Fragilariopsis* specimens. The
458 biogenic sedimentation is, however, lower than during spring which, coupled to increased
459 glacial runoffs, enables the concomitant settling of terrigenous particles from overflow glacial
460 plumes (Leventer *et al.*, 2002; Finocchiaro *et al.*, 2005). Events of high productivity during
461 summer dilute the terrigenous supply and are recorded as P sub-laminae. During autumn, light
462 level decreases, storm activity increases and sea ice returns, thus stimulating the formation of
463 *T. antarctica* that may even lead to Ta sub-laminae when the export is rapid.

464

465 5. 3. Interannual variability

466 While TSs represent snapshots of only a few years that may be lost in the centennial to
467 millennial climate variability, it is attractive to compare the two sequences in term of diatom
468 assemblages. The difference in terrigenous content between the two sections is not
469 conclusive. Section 5 from the Neoglacial period shows expanded spring laminations,
470 dominated by *F. curta*, and reduced summer laminations (Figure 3a). Section 13 from the
471 Hypsithermal period shows reduced spring laminations, dominated by *F. rhombica*, and
472 expanded summer laminations (Figure 3b). These findings demonstrate cooler conditions
473 during the period covered by TS 1-3 than during the period covered by TS 4-6, with late sea
474 ice break-up and early sea-ice return during the Neoglacial.

475 Superimposed on the climatic trends, a strong variability in lamination thickness and diatom
476 composition is encountered within each sequence of TS. In section 5, spring laminations of
477 years 1-5 appear much thicker than spring laminations of years 6-11 (Figure 3a) indicating
478 greater diatom productivity in relation to more stable and favourable environmental
479 conditions. This is further confirmed by the recurrence of transitional laminae at the
480 spring/summer transition in years 7-10, which possibly depicts enhanced wind activity during
481 this period. The occurrence of assemblage type B at the beginning of the spring season instead
482 of assemblage type A (Figure 3a) may result from more important injection of oligotrophic
483 warmer water (Stickley *et al.*, 2005) maybe resulting in earlier sea ice waning. In section 13,
484 diatom assemblages and succession are more complex during years 1-3 than during years 4-5.
485 Annual sedimentation rate is also reduced, especially because of thinner summer laminations,
486 and many sub-laminae are present during years 1-3 (Figure 3b). These findings again argue

487 for less stable conditions during this period that reduced the overall diatom productivity.
488 Lower productivity may also be related to lower nutrient input as shown by events of greater
489 CRS occurrence and higher silicification degree, maybe in relation to iron limitation
490 (Hutchins and Bruland, 1998), or to earlier return of sea ice in late summer as shown by the
491 Ta sub-laminae (Figure 3b).

492 While TSs represent snapshots of a few years in “cold” and “warm” periods, they argue for
493 strong environmental changes in nutrient supply and sea ice cover with a period of 3-5 years.
494 At these latitudes, sea ice seasonal waning and waxing is strongly dependant upon the
495 Antarctic Circumpolar Trough position (Enomoto and Ohmura, 1990). It is therefore
496 attractive to link the observed changes in environmental conditions to the Antarctic Dipole
497 that present a similar 4-5 years cyclicity (Yuan, 2004). Investigation of longer sequences of
498 sediment fabric may help to confirm or refute this hypothesis.

499

500 Conclusions

501 Preliminary investigation of core MD06-2301 from the Adélie Trough illustrates the presence
502 of laminated sedimentary layers that record seasonal and sub-seasonal diatom productivity
503 and lithic input. Light laminae are mainly biogenic layers with co-dominance of cryophilic
504 *Fragilariopsis* species and CRS. Light laminae correspond to the spring season. Dark
505 laminations show a mixture between terrigenous particles and complex diatom assemblages
506 dominated by *F. kerguelensis* and large centric species. Dark laminae represent the
507 summer/autumn season. Variations in lamination thickness and in diatom assemblage types
508 reveal a strong interannual variability that results from the interplay of sea ice, glacial runoff
509 and oceanic currents in response to interactions between the atmosphere, ocean and
510 cryosphere. These local to regional changes are possibly connected to the global sea ice cycle
511 around Antarctica via the Antarctic Dipole. Further investigations of longer sections will
512 provides a unique tool to document local to global Antarctic climate variability and cyclicity
513 during the Holocene period at the seasonal resolution.

514

515 Acknowledgements

516 We thank Eleanor Maddison, Jacques Giraudeau and William Fletcher for constructive
517 discussions. We also thank Jenny Pike, Amy Leventer and Lloyd Burckle whom helpful
518 reviews greatly improved the manuscript. We personally thank people from *Images X* (CADO)
519 cruise and from NSF-funded NBP0101 cruise for data and suggestions concerning the

520 D'Urville Trough. Financial support for this study was provided by TARDHOL project
521 through the national PNEDC Program (INSU-CNRS), and the Institut Paul Emile Victor
522 (IPEV). This is an EPOC contribution N°x.

523

524

525 References

526 **Amos, A. F.** 1987: RACER: physical oceanography of the western Bransfield Strait.
527 *Antarctic Journal of the United States* 22(5), 137-140.

528 **Armand, L.K., Crosta, X., Romera, O. and Pichon, J.J.** 2005: The biogeography of major
529 diatom taxa in Southern Ocean sediments: 1. Sea ice related species. *Palaeogeography,*
530 *Palaeoclimatology, Palaeoecology* 223, 93-126.

531 **Bahk, J. J., Yoon, H. I., Kim, Y., Kang, C. Y. and Bae, S. H.** 2003: Microfabric analysis of
532 laminated diatom ooze (Holocene) from the eastern Bransfield Strait, Antarctica Peninsula.
533 *Geosciences Journal* 7(2), 135-142.

534 **Beucher, C., Tréguer, P., Corvaisier, R., Hapette, A.M. and Elskens, M.** 2004: Production
535 and dissolution of biosilica, and changing microphytoplankton dominance in the Bay of Brest
536 (France). *Mar Ecol Prog Ser* 267, 57-69.

537 **Bindoff, N.L., Williams, G.D. and Allison, I.** 2001: Sea ice growth and water mass
538 modification in the Mertz Glacier Polynya during winter. *Annals of Glaciology* 33, 399-406.

539 **Bond, G., Cromer, B., Beer, J., Muscheler, R., Evans, M.N., Showers, W., Hoffman, S.,**
540 **Lotti-Bond, R., Hajdas, I. and Bonani G.** 2001: Persistent solar influence on North Atlantic
541 climate during the Holocene. *Science* 294, 2130-2136.

542 **Crawford, R.M.** 1995: The role of sex in the sedimentation of a marine diatom bloom.
543 *Limnology and oceanography* 40, 200-204.

544 **Crosta, X., Pichon, J. J., and Labracherie, M.** 1997: Distribution of *Chaetoceros resting*
545 *spores* in modern peri-Antarctic sediments. *Marine micropaleontology* 29, 238-299.

546 **Crosta, X., Crespin, J., Billy, I. and Ther, O.** 2005, Major factors controlling Holocene
547 $\delta^{13}\text{C}_{\text{org}}$ changes in a seasonal sea ice environment, Adélie Land, East Antarctica. *Global*
548 *Biogeochemical Cycles*, 19(4), GB4029, DOI: 10.1029/2004GB002426.

549 **de Menocal, P., Ortiz, J., Guilderson, T. and Sarnthein, M.** 2000: Coherent high- and low-
550 latitude climate variability during the Holocene warm period. *Science* 288, 2198-2202.

551 **Enomoto, H. and Ohmura, A.** 1990: The influences of atmospheric half-yearly cycle on the
552 sea ice extent in the antarctic. *Journal of Geophysical Research* 95 (C6), 9497-9511.

553 **Escutia, C., Warnke, D., Acton, G.D., Barcena, A., Burckle, L., Canals, M. and Frazee**
554 **C.S.** 2003: Sediment distribution and sedimentary processes across the Antarctic Wilkes Land
555 margin during the Quaternary. *Deep-Sea Research II* 50, 1481-1508.

556 **Finocchiaro, F., Langone, L., Colizza, E., Fontolan, G., Giglio, F. and Tuzzi, E.** 2005:
557 Record of the early Holocene warming in a laminated sediment core from Hallett Bay
558 (Northern Victoria Land, Antarctica). *Global and Planetary Change* 45, 193-206.

559 **Francus, P.** 1998: An image-analysis technique to measure grain-size variation in thin
560 sections of soft clastic sediments. *Sedimentary Geology* 121, 289-298.

561 **Francus, P., Keimig, F. and Besonen, M.** 2002: An algorithm to aid varve counting and
562 measurement from thin-sections. *Journal of Paleolimnology* 28, 283-286.

563 **Fryxell, G. A. and Hasle, G. R.** 1971: *Corethron criophilum* castracane: its distribution and
564 structure. *Antarctic Research Series* 17, 335-346.

565 **Garrison, D. L., Buck, K. R. and Fryxell, G. A.** 1987: Algal assemblages in Antarctic pack
566 ice and in ice-edge plankton. *Journal of Phycology* 23, 564-572.

567 **Harris, P. T.** 2000: Ripple cross-laminated sediments on the East Antarctic Shelf: Evidence
568 for episodic bottom water production during the Holocene? *Marine geology* 170, 317-330.

569 **Harris, P.T. and Beaman, R.J.** 2003: Processes controlling the formation of the Mertz Drift,
570 George Vth continental shelf, East Antarctica: evidence from 3.5kHz sub-bottom profiling and
571 sediment cores. *Deep-sea Research II* 50, 1463-1480.

572 **Hodell, D. A., Shemesh, A., Crosta, X., Kanfoush, S., Charles, C. and Guilderson, T.**
573 2001: Abrupt cooling of Antarctic surface waters and sea ice expansion in the South Atlantic
574 sector of the Southern Ocean at 5000 cal yr BP. *Quaternary research* 56, 191-198.

575 **Huntley, M. E., Niiler, P., Holm-Hansen, O. and Karl, D. M.** 1987. RACER: An inter-
576 disciplinary field study. *Antarctic Journal of the United States* 22, 135-137.

577 **Hutchins, D. A. and Bruland, K. W.** 1998: Iron-limited diatom growth and Si:N uptake
578 ratios in a coastal upwelling regime. *Nature* 393, 561-564.

579 **Ingólfsson, O., Hjort, C., Berkman, P.A., Björck, S., Colhoun, E., Goodwin, I.D., Hall,**
580 **B., hirakawa, K., Melles, M., Möller, P. and Prentice, M.L.** 1998: Antarctic glacial history
581 since the last glacial maximum: an overview of the record on land. *Antarctic Science* 10, 326-
582 344.

583 **Jansen, J. H. F., Van der Gaast, S. J., Koster, B. and Vaars, A. J.** 1998: CORTEX, a
584 shipboard XRF-scanner for element analyses in split sediment cores. *Marine Geology* 151,
585 143-153.

586 **Jones, P. D., Marsh, R., Wigley, T. M. L. and Peel, D. A.** 1993: Decadal timescale links
587 between Antarctic Peninsula ice core oxygen-18 and temperature. *Holocene* 3, 14-26.

588 **Kemp, A. E. S., Pearce, R. B., Koizumi, I., Pike, J. and Rance, S. J.** 1999: The role of mat
589 forming diatoms in formation of the Mediterranean Sapropels. *Nature* 398, 57-61.

590 **Kemp, A.E.S., Pike, J., Pearce, R.B. and Lange, C.B.** 2000: The “fall dump”: a new
591 perspective on the role of a shade flora in the annual cycle of diatom production and export
592 flux. *Deep-Sea Research II* 47, 2129-2154.

593 **King, J. C. and Turner, J.** 1997: Antarctic Meteorology and Climatology. *Cambridge*
594 *Atmospheric and Space Science Series*, Cambridge University Press, 409pp.

595 **King, J. C., Turner, J., Marshall, G. L., Connolley, W. M. and Lachlan-Cope, T. A.** 2003:
596 Antarctic Peninsula climate variability and its causes as revealed by analysis of instrumental
597 records. *In Antarctic Peninsula Climate Variability* 79, 12-1 – 12-4.

598 **Leventer, A. and Dunbar, R. B.** 1987: Diatom flux in McMurdo Sound, Antarctica. *Marine*
599 *Micropaleontology* 12, 49-64.

600 **Leventer, A.** 1991: Sediment trap diatom assemblages from the northern Antarctic Peninsula
601 region. *Deep Sea Research* 38, 1127-1143.

602 **Leventer, A.** 1992: Modern distribution of diatoms in sediments from the George V coast,
603 Antarctica. *Marine Micropaleontology* 19, 315-332.

604 **Leventer, A., Domack, E., Barkoukis, A., McAndrews, B. and Murray, J.** 2002:
605 Laminations from the Palmer Deep: A diatom-based interpretation. *Paleoceanography* 17, 1-
606 15.

607 **Leventer, A., Domack, E., Dunbar, R., Pike, J., Stickley, C., Maddison, E., Brachfeld, S.,**
608 **Manley, P., and McClennen, C.** East Antarctic Margin Marine Sediment Record of
609 Deglaciation, *GSA Today*, submitted.

610 **Maddison, E. J., Pike, J., Leventer, A. and Domack, E. W.** 2005: Deglacial seasonal and
611 sub-seasonal diatom record from Palmer Deep, Antarctica. *Journal of Quaternary Science* 20,
612 435-446.

613 **Maddison, E. J.** 2005: Seasonally laminated Late Quaternary Antarctic sediments. Ph. D.
614 thesis, Cardiff University, 218 pp.

615 **Masson, V., Vimeux, F., Jouzel, J., Morgan, V., Delmotte, M., Ciais, P., Hammer, C.,**
616 **Johnsen, S., Lipenkov, Y., Mosley-Thompson, V. E., Petit, J. -R., Steig, E. J., Stievenard,**
617 **M. and Vaikmae R.** 2000: Holocene climatic variability in Antarctica: what can be inferred
618 from 11 ice core isotopic records? *Quaternary Research* 54, 348-358.

619 **Migeon, S., Weber, O., Faugeres, J. –C. and Saint-Paul, J.** 1999: SCOPIX: A new X-ray
620 imaging system for core analysis. *Geo-Marine Letters* 18, 251-255.

621 **McMinn, A. and Hodgson, D.** 1993: Seasonal phytoplankton succession in Ellis Fjord,
622 eastern Antarctica. *J. Plankton. Res.* 15, 925-938.

623 **NGICP members.** 2004: High-resolution record of Northern Hemisphere climate extending
624 into the last interglacial period. *Nature* 431, 147-151.

625 **Nielsen, S. H. H., Koç, N. and Crosta X.** 2004: Holocene climate in the Atlantic sector of the
626 Southern Ocean: Controlled by insolation or oceanic circulation? *Geology* 32, 317-320.

627 **Pike, J., Moreton, S. G. and Allen, C. A.** 2001: Data report: Microfabric analysis of
628 postglacial sediments from Palmer Deep, Western Antarctic Peninsula. In: Barker, P. F.,
629 Camerlenghi, A., Acton, G. D., Ramsay, A. T. S. (Eds), Proc. ODP, *Sci. Res.* 178, 1-17
630 [online]. Available from World Wide Web:
631 http://www.odp.tamu.edu/publications/178_SR/VOLUME/CHAPTERS/SR178_18.PDF
632 [cited 2005-April 9].

633 **Presti, M., De Santis, L., Buseti, M. and Harris, P.T.** 2003: Late Peistocene and Holocene
634 sedimentation on the George V Continental Shelf, East Antarctica. *Deep-Sea Research II* 50,
635 1441-1461.

636 **Rathburn, A. E., Pichon, J. -J., Ayress, M. A., and De Deckker, P.** 1997. Microfossil and
637 stable-isotope evidence for changes in the late Holocene paleoproductivity and
638 paleoceanographic conditions in the Prydz Bay region of Antarctica. *Palaeogeography,*
639 *Palaeoclimatology, Palaeoecology* 131, 485-510.

640 **Riaux-Gobin, C., Poulin, M., Prodon, R. and Treguer, P.** 2003: Land-fast ice microalgal
641 and phytoplanktonic communities (Adélie land, Antarctica) in relation to environmental
642 factors during ice break-up. *Antarctic Science* 15 (3), 353-364.

643 **Rignot, E. and Jacobs, S. S.** 2002: Rapid Bottom Melting Widespread near Antarctic Ice
644 Sheet Grounding Lines. *Science* 296, 2020-2023.

645 **Saporta, G.** 1990: Probabilités analyse des données et statistique. Editions technip.

646 **Schweitzer, P.N.** 1995: Monthly averaged polar sea ice concentration. *U.S. Geological*
647 *Survey Digital Data Series*, Virginia.

648 **Stammerjohn, S. E., Drinkwater, M. R., Smith, R.C. and Liu, X.** 2003: Ice-atmosphere
649 interactions during sea-ice advance and retreat in the western Antarctic Peninsula region.
650 *Journal of Geophysical Research* 108, 3329 pp. DOI: 10.1029/2002JC001543:27 .1-27 .15.

651 **Stickley, C.E., Pike, J., Leventer, A., Dunbar, R.B., Domack, E.W., Brachfeld S.A.,**
652 **Manley, P. and McClennan, C.** 2005: Deglacial ocean and climate seasonality in laminated

653 diatom sediments, Mac Robertson Shelf, East Antarctica Margin. *Palaeogeography,*
654 *Palaeoclimatology, Palaeoecology* 227, 290-310.

655 **Taylor, S. R.** and **Mc lennan, S. M.** 1985: The continental Crust: Its Composition and
656 Evolution. *Blackwell Science*, 312 pp.

657 **Van Bennekom, A. J., Jansen, J. H. F., Van der Gaast, S. J., Van Iperen, J. M.** and
658 **Pieters, J.** 1989: Aluminium-rich opal: An intermediate in the preservation of biogenic silica
659 in the Zaire (Congo) deep-sea fan. *Deep-Sea Research* 36, 173-190.

660 **Yarincik, K. M.** and **Murray, R. W.** 2000: Climatically sensitive eolian and hemipelagic
661 deposition in the Cariaco Basin, Venezuela, over the past 578,000 years: Results from Al/Ti
662 and K/Al. *Paleoceanography* 15, 210-228.

663 **Yuan, X.** 2004: ENSO-related impacts on Antarctic sea ice: A synthesis of phenomenon and
664 mechanisms. *Antarctic Science* 16, 415-425.

665 **Zaragosi, S., Bourillet, J-F., Eynaud, F., Denhard, B., Van Toer, A., and Lanfumey, V.**
666 (submitted). The impact of the last European deglaciation on the Bay of Biscay turbidite
667 systems. *Geomarine Letters*.

668 **Zielinski, U.** and **Gersonde, R.** 1997: Diatom distribution in Southern Ocean surface
669 sediments (Atlantic sector): Implications for paleoenvironmental reconstructions.
670 *Palaeoceanography, Palaeoclimatology, Palaeoecology* 129, 213-250.

671
672
673
674
675
676
677
678
679
680
681
682
683
684
685
686

687 Figure captions

688

689 **Figure 1.** Location of core MD03-2601, limit of summer sea-ice cover (Schweitzer, 1995),
690 location of glaciers and ice-streams (Massom *et al.*, 1998; Escutia *et al.*, 2003), detail of
691 oceanographic currents and different water masses (Harris and Beaman, 2003). DDU:
692 Dumont d'Urville Base; ACC: Antarctic Coastal Current; MCDW: Modified Circumpolar
693 Deep Water; HSSW: High Salinity Shelf Water. Winter sea ice covers the whole oceanic area
694 encompassed by the map.

695 **Figure 2.** Mean number of laminations per 10 cm intervals (dashed line) and thickness of
696 dark (black line) and light (grey line) and laminations versus depth. Laminae thicknesses are
697 smoothed with a 50 cm running average. Core sections, climatic periods and ¹⁴C dates are
698 reported on the top. The location of the studied sections 5 and 13 is represented by shaded
699 zones.

700 **Figure 3.** Schematic log of lamination and sub-lamination distribution in section 5 (a) and in
701 section 13 (b). Location of the centimetric scale thin sections, and number of annual couplets
702 are reported on the left side. Pie-charts illustrate the relative abundance of the various diatom
703 groups from centimetric scale diatom census counts in section 5 (a) and 13 (b).

704 **Figure 4.** Location of the investigated sections on positive X-ray radiographs, thin sections
705 and photomosaics for section 5 (a) and section 13 (b). Three thin sections (TS) were taken
706 from each section. Two photomosaics (PM) were analysed in TS1 from section 5 while five
707 photomosaics were analysed in the three TS from section 13. In each section, Ti content is
708 visualized by the black curve. In the photomosaics, Ti content is represented by the grey
709 curve with white points whereas the grain number per mm is illustrated by the white curve.
710 Types of laminae and couplet succession is shown on the right of TS following the
711 nomenclature depicted in figure 3.

712 **Figure 5.** Photograph board illustrating various diatom assemblage types. Photographs 1-3
713 and 5-6 show, respectively, typical light/biogenic laminae and dark/terrigenous laminae
714 assemblages. Photograph 7 illustrates two types of sub-laminae. Photographs 4 and 8 compare
715 two different degrees of silicification on two diatom species.

716 **Figure 6.** Conceptual model for the deposition of the different laminations and sub-laminae
717 recorded in core MD03-2601 for the spring season (a) and the summer-autumn season (b).

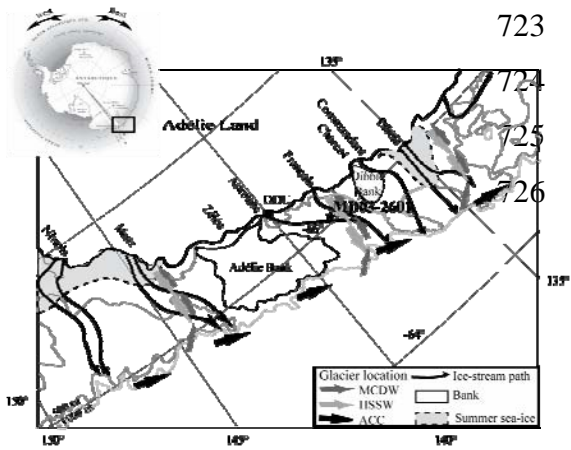
718

719

720

721 **Figure 1**

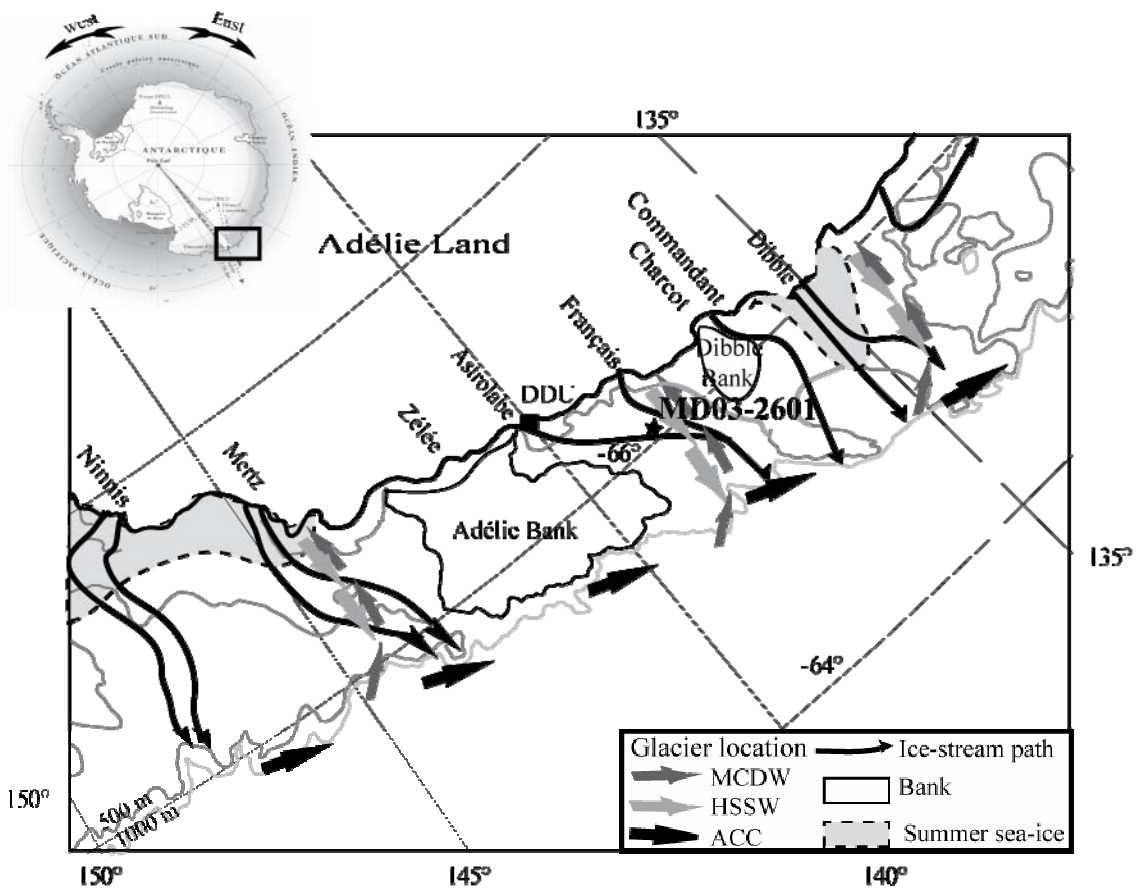
722



727

728

729



730

731

732

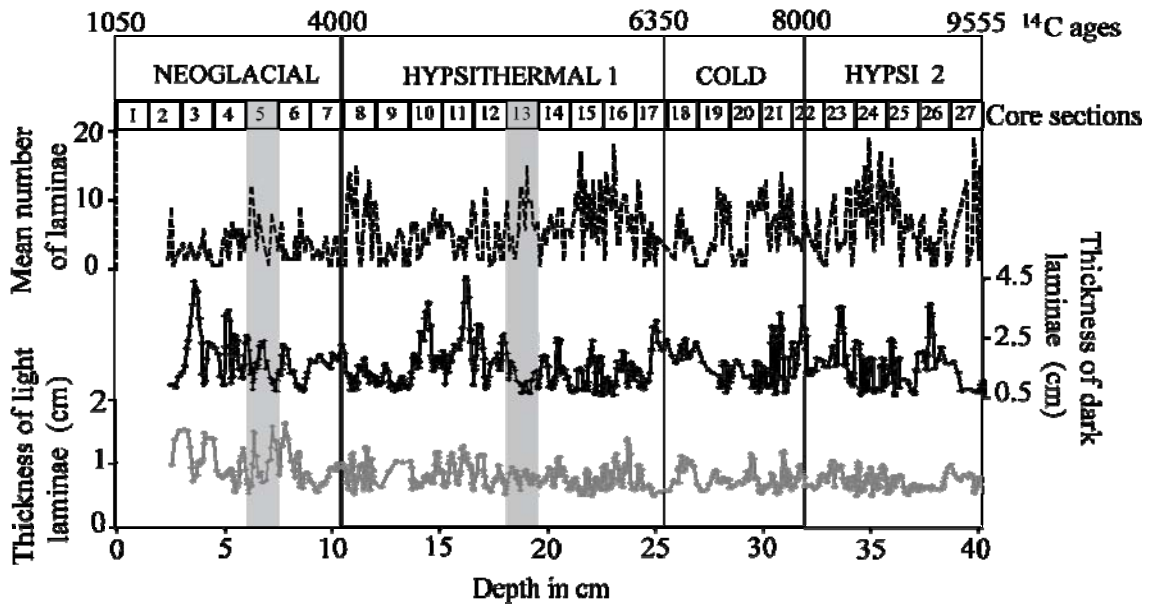
733

734 Not sized, for peer review

735

736 Figure 2

737



738

739

740 Sized to 2 columns

741

742

743

744

745

746

747

748

749

750

751

752

753

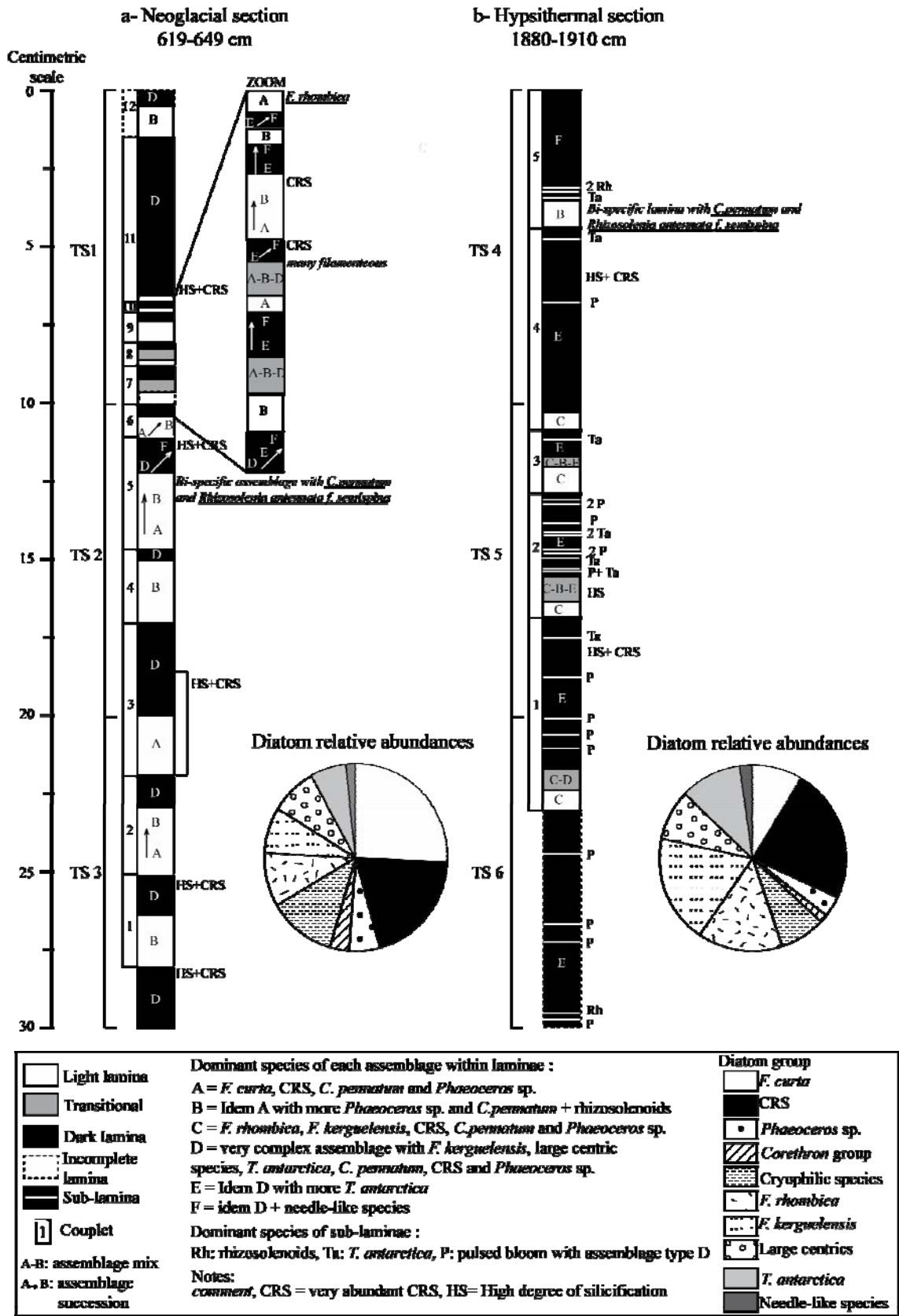
754

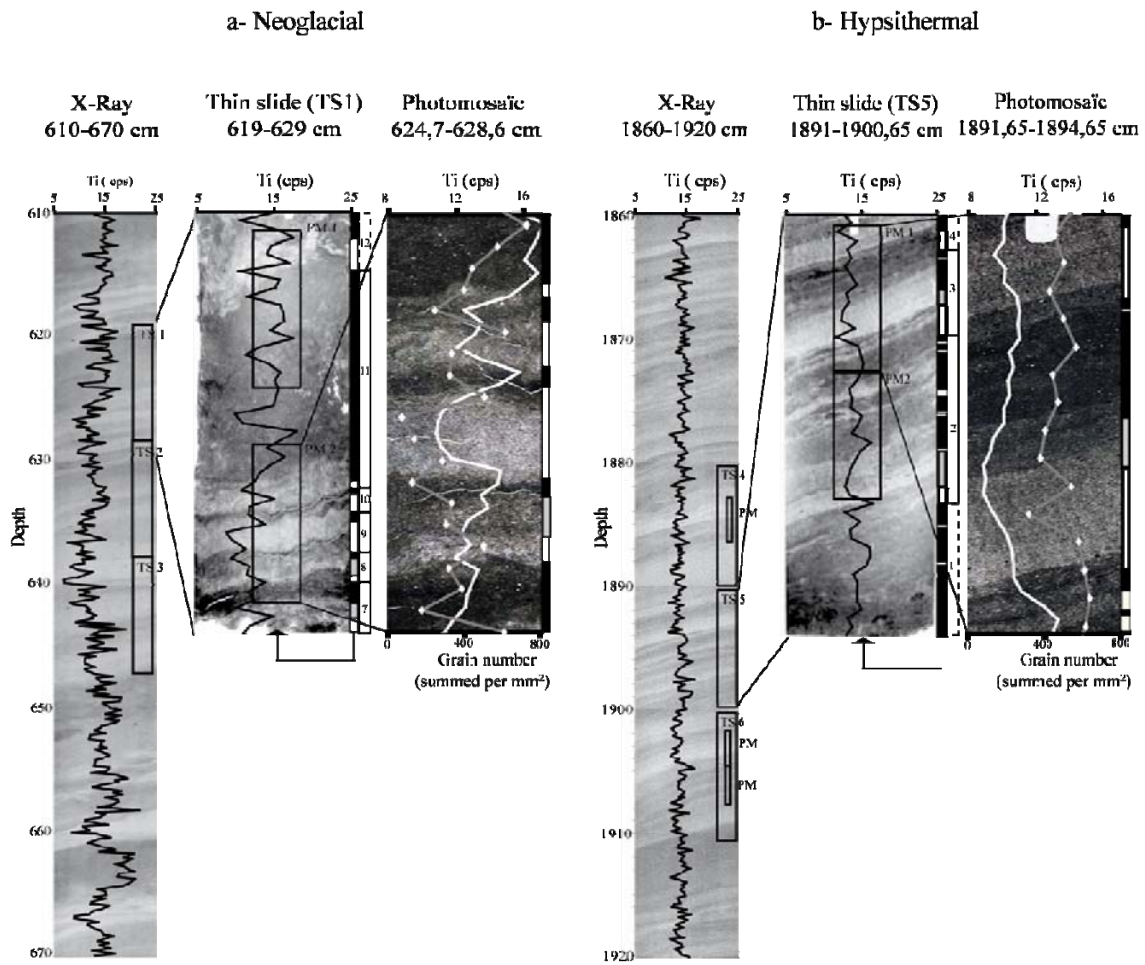
755

756

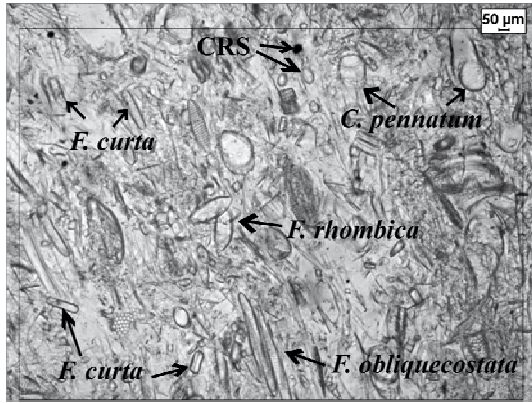
757

758

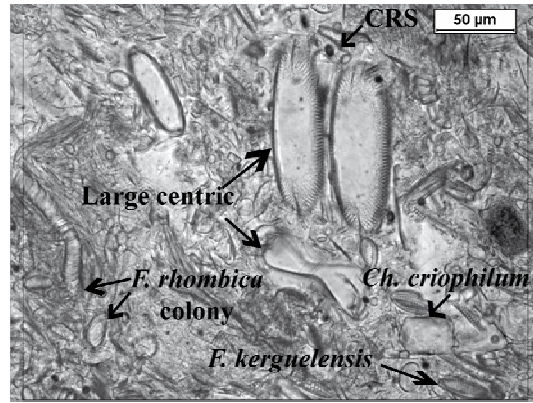




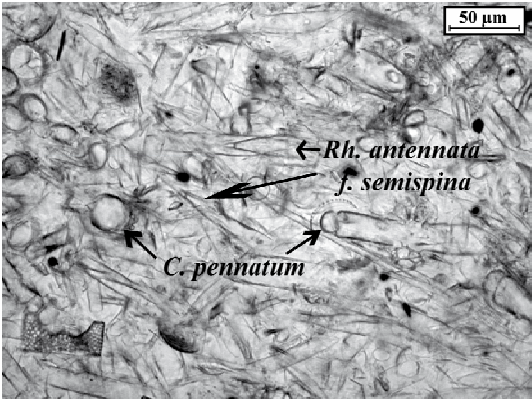
- 764 Light lamina Transitional lamina Dark lamina Dark lamina - light sub-lamina Couple? Incomplete couple?
- 765
- 766
- 767
- 768
- 769
- 770
- 771
- 772
- 773
- 774
- 775
- 776
- 777
- 778



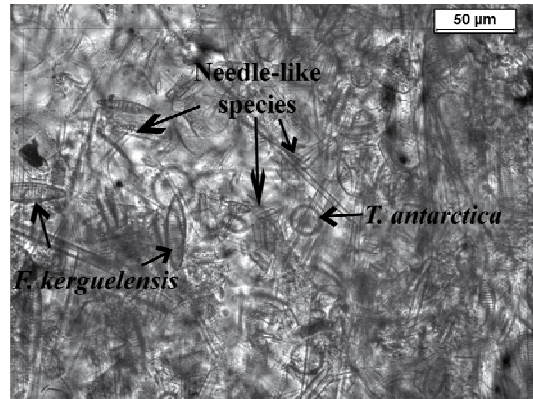
1. A type



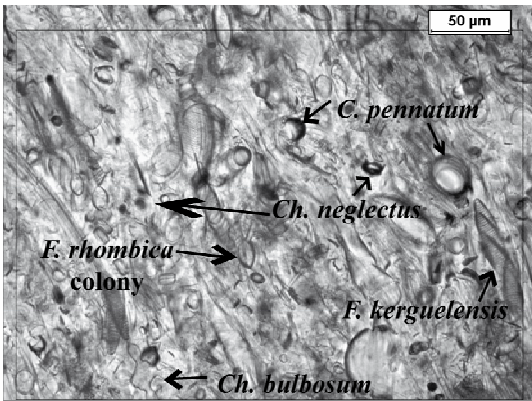
5. D type



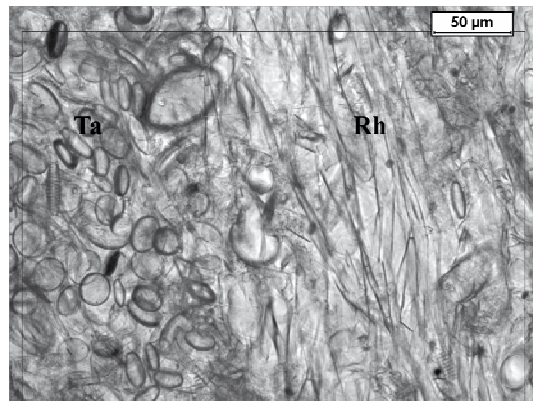
2. B type



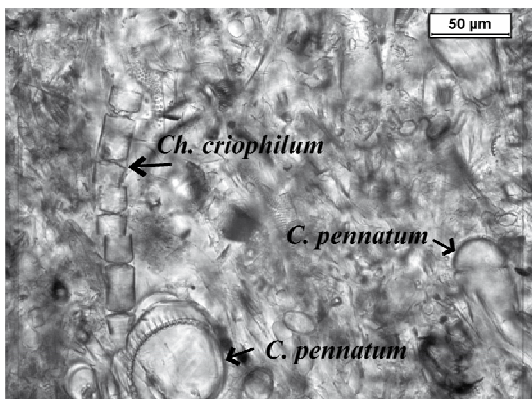
6. F type



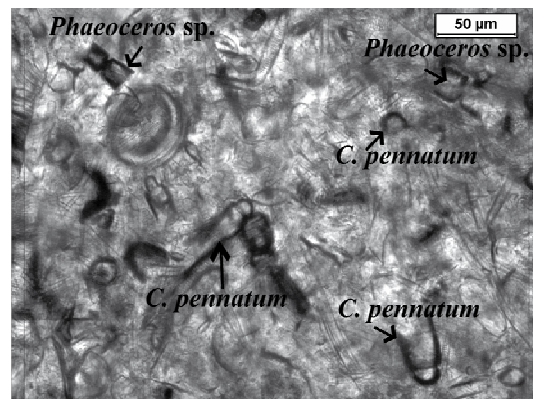
3. C type



7. Ta and Rh sub-laminae

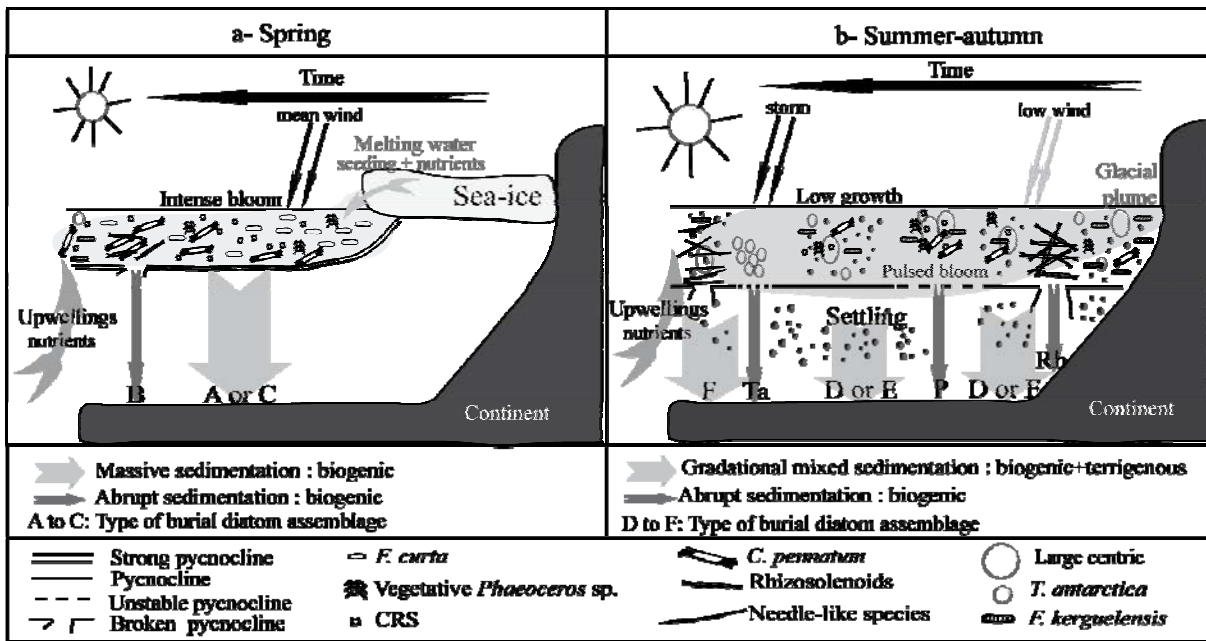


4. Low silicification degree



8. High silicification degree

781 Figure 6



782
783
784
785
786
787